Miner Petrol (2013) 107:501–515
DOI 10.1007/s00710-012-0250-6

ORIGINAL PAPER

Topotactic formation of ferrisicklerite from natural triphylite under hydrothermal conditions

Peter Schmid-Beurmann · Luisa Ottolini · Frédéric Hatert · Thorsten Geisler · Magdalena Huyskens · Volker Kahlenberg

Received: 20 June 2012 / Accepted: 12 November 2012 / Published online: 1 December 2012

Abstract The topotactic oxidation and delithiation reaction from triphylite, $Li(Fe,Mn)PO_4$, leading to ferrisicklerite, $Li_{<1}(Fe^{3+},Mn^{2+})PO_4$, was investigated under hydrothermal conditions. A cuboid cut from a triphylite single-crystal (Palermo Mine, New Hampshire, USA) with the composition $Li_{0.93(3)}(Fe^{2+}_{0.733(6)},Fe^{3+}_{0.015(1)},Mn^{2+}_{0.210(4)},Mg_{0.063(2)})_{1.021(8)}P_{1.00(2)}O_4$ in addition with ground bulk material were treated with $KMnO_4$ and 30 % H_2O_2(aq) as oxidizing agent in a 0.1 N hydrochloric acid solution in the temperature range between 60 and 200 °C. At 120 °C a rim of 0.1 mm thickness of ferrisicklerite had formed around the core of unreacted triphylite. The sharp reaction boundary was clearly visible, due to the reddish brown absorption colors of ferrisicklerite, compared to colorless triphylite. Using single-crystal X-ray diffraction (XRD), secondary ion mass spectrometry (SIMS), electron probe micro-analysis (EPMA) and ^{57}Fe-Mössbauer spectroscopy the product ferrisicklerite was characterized and its composition determined as $Li_{0.30(7)}(Fe^{2+}_{0.049(1)}Fe^{3+}_{0.65(2)}Mn^{2+}_{0.218(5)}Mg_{0.062(2)})_{0.98(1)}P_{1.01(3)}O_4$, with unit cell parameters a=4.795(1), b=9.992(4), and c=5.886(2) Å. EPMA investigations across the reaction boundary showed no changes in the concentrations of Fe, Mn, Mg, and P. In contrast, SIMS measurements clearly proved the delithiated state of the ferrisicklerite product. Polarization microscopy revealed that the orientation of the ferrisicklerite rim was the same as that of the original triphylite single-crystal, confirming the strictly topotactic character of the reaction.

Editorial handling: A. Beran

P. Schmid-Beurmann (✉) · M. Huyskens
Institut für Mineralogie, Universität Münster, Corrensstr. 24,
48149 Münster, Germany
e-mail: psb@uni-muenster.de

L. Ottolini
C.N.R.- Istituto di Geoscienze e Georisorse (IGG), Unità di Pavia,
Via A. Ferrata 1,
27100 Pavia, Italy

F. Hatert
Laboratoire de Minéralogie, Département de Géologie,
Université de Liège, Bâtiment B18,
4000 Liège, Belgium

T. Geisler
Universität Bonn, Steinmann-Institut für Geologie,
Mineralogie und Paläontologie, Poppelsdorfer Schloß,
33115 Bonn, Germany

V. Kahlenberg
Universität Innsbruck, Institut für Mineralogie und Petrographie,
Innrain 52,
6020 Innsbruck, Austria

Introduction

Minerals of the triphylite-lithiophilite solid solution series are widespread primary (magmatic) phases in granitic pegmatites. In later stages of pegmatitic evolution they are the source of several secondary mineral associations which can be formed by metasomatic reactions under decreasing temperature (Moore 1971; Fransolet et al. 1986). Up to now the physico-chemical conditions of such processes cannot be confidently specified. Attempts to overcome this problem were recently started by investigating the stability properties of primary phosphates like alluaudite in hydrothermal experiments under controlled oxygen fugacities and by implementing the Na-in-triphylite geothermometer (Hatert et al. 2006, 2011). In this paper we focus on the oxidation reaction by which the triphylite-lithiophilite solid solutions progressively

transform to the Li-depleted minerals ferrisicklerite-sicklerite and heterosite-purpurite, according to the so-called Mason-Quensel sequence (Quensel 1937; Mason 1941; Fransolet et al. 2004):

triphylite − lithiophilite ⇒	ferrisicklerite − sicklerite ⇒	heterosite − purpurite.
$Li(Fe^{2+}_{x}Mn^{2+}_{1-x})PO_4$	$Li_{1-x}(Fe^{3+}_{x}Mn^{2+}_{1-x})PO_4$	$\square(Fe^{3+}_{x}Mn^{3+}_{1-x})PO_4$

These reactions are topotactic as the three minerals are isotypic and crystallize in the olivine structure type (e.g. Finger and Rapp 1969; Losey et al. 2004; Alberti 1976; Eventoff et al. 1972; Bjoerling and Westgren 1938) and there is a strong orientational relationship between educt and product as they show the same extinction behavior under crossed polarizers. In triphylite the M1 and M2 octahedral positions are occupied by Li^+ and Fe^{2+}; the latter often replaced by Mn^{2+}. During the first step of the reaction the divalent iron of the triphylite-lthiophilite solid solution is oxidized to the ferric state. In order to achieve charge balance an equivalent amount of Li^+ in M1 is extracted from the crystal. So a member of the ferrisicklerite-sicklerite solid solution is formed. In the second step of the reaction Mn^{2+} is oxidized and a completely Li-free member of the sequence heterosite-purpurite is formed. It has been suggested that ferrisicklerite-sicklerite develops metasomatically under hydrothermal conditions, whereas the conditions of the second step, i.e., the formation of heterosite-purpurite, range from hydrothermal conditions to weathering (Keller and von Knorring 1989; Fransolet et al. 1986; Fontan et al. 1976). Independently, both replacement reactions indicate an increase of the oxidation potential of the environment. To the best of our knowledge, the synthesis of oxidized members of the Mason-Quensel sequence, such as ferrisicklerite and heterosite, under hydrothermal conditions has never been reported. Such investigation would be a first step to elucidate the formation conditions and the mechanism of this topotactic reaction leading to this suite of phosphate minerals and therefore would be a contribution to the characterization of the physico-chemical conditions of phosphate mineral formation in granitic pegmatites. In this paper, we report a study on the hydrothermal oxidation reaction of natural triphylite single-crystals and synthetic lithiophilite, $LiMnPO_4$, to form ferrisicklerite, and their phase characterization by X-ray diffraction, EPMA, SIMS and ^{57}Fe-Mössbauer spectroscopy.

Methods

Preparation of starting material and hydrothermal experiments

As starting materials a natural triphylite, $Li(Fe,Mn)PO_4$, specimen as well as synthetic lithiophilite, $LiMnPO_4$, were used. The natural triphylite (Palermo Mine, New Hampshire, USA, sample# 9706.41 given by Paul Keller, Stuttgart) was used in form of powder and polished cuboids with edge lengths of 2.5 mm. The powder was prepared from the same triphylite sample as the cuboids by milling the sample in a ball mill and then sieving it to a grain size between 125 and 250 μm. Lithiophilite, $LiMnPO_4$, was prepared from a homogenized stoichiometric mixture of Li_3PO_4, $Mn_2P_2O_7$ and MnO (Alfa A06F05, >99.5 %). For synthesis of Li_3PO_4 stoichiometric amounts of Li_2CO_3 (Merck # 5680, > 99 %) and $NH_4H_2PO_4$ (Fluka # 09709>99.5 %) were homogenized in a ball mill, pressed to pellets, and then heated in a Pt-crucible at a temperature of 700 °C for 2 days. $Mn_2P_2O_7$ was synthesized from a stoichiometric mixture of MnO and $NH_4H_2PO_4$. According to X-ray powder diffraction analyses all products were single-phase Li_3PO_4 (lithiophosphate, PDF # 15–760), $Mn_2P_2O_7$ (PDF# 29–891) and $LiMnPO_4$ (lithiophilite, PDF# 74–375).

Hydrothermal experiments without oxygen buffering under authigenic pressures at temperatures between 60 and 200 °C were performed using steel autoclaves with inner Teflon© vessels (Institut für Mineralogie, University of Münster) . Around 25–50 mg of starting material, either as cuboids or powder, were placed together with 1 ml of 0.1 N hydrochloric acid into the Teflon© vessels, the latter having a total volume of 3 cm^3. $KMnO_4$ or 30 % H_2O_2(aq) were added as oxidant agent. After closure, the autoclaves were weighted and then placed into a furnace where they were kept between 7 and 28 days (Table 1). After the experiments the autoclaves were checked for weight loss and the remaining solutions were separated from the solid and stored in plastic tube vacuoles. The solid was washed with distilled water and then dried in a furnace at a temperature of 50 °C.

Single-crystal X-ray structure determination

Single-crystal intensity measurements of triphylite and ferrisicklerite crystals were performed using a STOE imaging plate detector system IPDS (Institut für Mineralogie und Petrographie, University of Innsbruck) at room temperature. Parameters of the data collections and structure refinements are summarized in Table 2. Triphylite as well as synthetic ferrisicklerite have the orthorhombic Laue symmetry *mmm*. Analysis of reflection conditions resulted in space group *Pmnb* (space group no. 62) Data reduction including

Table 1 Conditions of hydrothermal oxidation and delithiation experiments of natural triphylite and synthetic lithiophilite

Run	Sample	Mass [mg]	T [°C]	t [d]	Oxidant agent [d]	Products and PDF #
	Triphylite				30%H_2O_2(aq) [µl]	
Tri-116	bulk[a,b]	25	200	28	21	tavorite PDF 10–424 barbosalite PDF 85–1728 triphylite PDF 40–1499,
Tri-115	bulk[a,b]	25	170	28	21	triphylite PDF 40–1499, giniite ferric synth 45–1436
Tri-117	bulk[a,b]	25	120	28	21	triphylite PDF 40–1499, giniite ferric synth 45–1436
MH 1.1	bulk[a,b]	51.36	100	7	21	triphylite PDF 40–1499 giniite ferric synth 45–1436
MH 1.2	bulk[a,b]	49.99	80	7	21	triphylite PDF 40–1499 ferrisicklerite PDF 29–808
Tri-118	bulk[a,b]	25	70	28	21	triphylite PDF 40–1499 ferrisicklerite PDF 29–808
MH 1.3	bulk[a,b]	51.23	60	7	21	triphylite PDF 40–1499 ferrisicklerite PDF 29–808
					$KMnO_4$ [mg]	
Tri-87	cuboid[a] (2.5 mm)^3	53.5	120	8	21	cube with, - outer rim: opaque Mn-Ox - inner rim: redbrown ferrisicklerite - core: colorless triphylite
MH 2.1	bulk[a,b]	50.3	170	7	21	ferrisicklerite PDF 29–808
Tri-77	bulk[a,b]	50.8	120	8	20.2	ferrisicklerite PDF 29–808
MH 2.3	bulk[a,b]	50.7	80	7	21	ferrisicklerite PDF 29–808
Tri-121	bulk[a,b]	50.0	70	17	21.0	ferrisicklerite PDF 29–808
Tri-74	$LiMnPO_4$[c]	49.7	120	28	10.5	lithiophilite PDF 33−803

[a] natural triphylite from Palermo Mine, N.H. USA (#9706.41 given by Paul Keller, Stuttgart). [b] ground material with grain size of 125–250 µm. [c] synthetic lithiophilite powder. [d] admixed to 1 ml 0.1 N HCl

intensity integration, background as well as Lorentz and polarization correction was performed with the STOE XRED software package. Furthermore, the irregular shapes of the crystal fragments were approximated by external faces and a face absorption correction was applied.

The structures of both natural triphylite (9706.41) as well as synthetic ferrisicklerite (Tri-77) were solved by direct methods with the program SIR92 (Altomare et al. 1992) in order to obtain a model that is unbiased from any pre-assumptions. Structure determination was completed by difference Fourier calculations providing the starting parameters for the least-squares refinements performed with the program SHELX-97 (Sheldrick 1997). X-ray scattering factors for the cations in their respective valence state (Li^+, Fe^{2+}, Fe^{3+}) together with real and imaginary anomalous-dispersion corrections were taken from the *International Tables for X-Ray Crystallography* (Ibers and Hamilton 1974). The values for O^{2-} were taken from Hovestreydt (1983). For better comparison with previous investigations (Losey et al. 2004) the results were transformed to the *Pbnm* setting of space group no. 62 (Table 3).

X-ray powder diffraction (XRPD)

For phase characterization of the products, X-ray powder diffraction patterns were recorded using a SIEMENS D5000 diffractometer (Cu-K_α radiation, secondary beam graphite monochromator, Institut für Geowissenschaften, University of Kiel). The operating conditions were 40 kV and 30 mA. Qualitative phase analyses were done using the EVA-package of Diffrac^{Plus} software (BRUKER, Germany). Rietveld refinement was performed using the FULLPROF SUITE 2005 (Rodriguez-Carvajal 2005). As starting parameters crystal structural data for triphylite, ferrisicklerite and lithiophilite were taken from Losey et al. (2004); Alberti (1976) and Yonemura et al. (2004). The results are given in Tables 4 and 5, as well as in Fig. 1.

^{57}Fe-Mössbauer spectroscopy

^{57}Fe-Mössbauer spectra of synthetic triphylite and synthetic ferrisicklerite were recorded using a ~0.5 GBq ^{57}Co/Rh source at room temperature in combination with a

Table 2 Data collection and single-crystal structure refinement parameters

(A)	Crystal data	Triphylite 9706.41	Synthetic ferrisicklerite, Tri-77
	Temperature	293(2) K	293(2)
	Space group	*Pbnm*	*Pbnm*
	Z	4	4
	μ (mm^{-1})	5.518	5.512
	Crystal dimensions	180×120×70 μm	Longest diameter 200 μm
(B)	Intensity measurements		
	Diffractometer	Stoe-IPDS	
	Monochromator	graphite	
	Radiation	Mo$K\alpha$. λ=0.71073 Å	
	X-Ray power	50 kV, 40 mA	
	Rotation width in ϕ (°)	2	
	No. of exposures	180	
	Irradiation time/exposure (min)	3	
	θ-range	3.94–26.68	4.08–26.70
	Reflection range	$\|h\|\leq 9$; $\|k\|\leq 13$; $\|l\|\leq 5$	$\|h\|\leq 7$; $\|k\|\leq 12$; $\|l\|\leq 6$
	No. of measured reflections	4039	3150
	No. of unique reflections in *mmm*	337	328
	R_{int} in 2/*m* after abs. corr.	0.0403	0.0339
	No. of obs. reflections (I>2σ(I))	797	755
(C)	Structure refinement		
	No. of refined parameters	41	42
	R1(F_o>2σ(F_o)); R1(all data)	0.0230; 0.0230	0.0282; 0.0292
	wR2 (F_o>2σ(F_o))	0.0623	0.078
	Extinction coefficient	0.046(5)	0.013(4)
	Goodness of fit	1.351	1.38
	Final $\Delta\rho_{min}$ ($e/Å^3$)	−0.322	−0.459
	Final $\Delta\rho_{max}$ ($e/Å^3$)	0.468	0.394
	$R1=\Sigma\|\|F_o\|-\|F_c\|\|/\Sigma\|F_o\|$	$wR2=\Sigma(w(\|F_o^2-F_c^2)^2)/\Sigma(w(F_o^2)^2))^{½}$	
	$w=1/(\sigma^2(F_o^2)+(aP)^2)$	$P=(2F_c^2+\max(F_o*2*.0))/3$	

constant-acceleration spectrometer (Institut für Geowissenschaften, University of Kiel). For absorber preparation about 5 to 8 mg of sample were diluted in 200 mg of avicel as a matrix and pressed to pellets with 0.5 inch diameter. Lorentzian line profiles were fitted to the spectra (Fig. 2). The isomer shifts are given relative to ^{57}Fe in α-Fe (Table 6).

Electron probe micro-analysis

Starting materials and experimental run products were quantitatively analysed by EPMA using a JEOL JXA 8900 Superprobe (Institut für Mineralogie, University of Münster) operated at 15 kV acceleration voltage and 15 nA beam current. The standards used were jadeite (Na), diopside (Si, Ca), apatite (P), rhodonite (Mn), olivine (Mg), sanidine (K), fayalite (Fe), willemite (Zn), rutile (Ti). The ZAF correction procedure was applied to correct matrix effects. Results are given in Tables 7 and 8.

SIMS

The SIMS measurements were done with a Cameca IMS 4f ion microprobe installed at CNR-IGG, Pavia (Italy), following a procedure similar to that described in Hatert et al. (2011). We used a 12.5 kV accelerated $^{16}O^-$ primary-ion beam with a a very low current of~0.1 nA, corresponding to a beam diameter on the order of 5 μm. The samples were polished, washed in an ultrasonic tank with ethanol, and Pt coated (400 Å thickness) before analysis. Secondary-ion signals of the isotopes $^6Li^+$, $^{31}P^+$ and $^{57}Fe^+$ were detected at the electron multiplier. Acquisition times were 3 s for Li and P (each), and 6 s for Fe over 3 cycles. Analyses were done under *steady-state* sputtering conditions after 360 s sputtering using~75–125 eV secondary ions. As it was demonstrated (Ottolini et al. 1993, 2002 and references therein), the choice of medium-to-high-energy (*energy filtering*) secondary ions

Table 3 Structural data and lattice parameters (space group *Pbnm*) from single-crystal investigations of triphylite and ferrisicklerite

		Natural triphylite Trip79 (Losey et al. 2004)	Natural triphylite 9706.41 this work	Natural ferrisicklerite (Alberti 1976)	Ferrisicklerite Tri-77 this work
Li, M1	*x*, *y*, *z*	0, 0, 0	0, 0, 0	0, 0, 0	0, 0, 0
	B	0.78(6)	0.79(8)	2.0(4)	0.78*
	occ	1	1	0.32(3)	0.32(2)
Fe, Mn, M2	*x*	0.97436(6)	0.9746(1)	0.96361(9)	0.9633(2)
	y	0.2820(3)	0.2820(1)	0.27815(4)	0.2770(1)
	z	¼	¼	¼	¼
	B	0.592(5)	0.87(8)	0.63(1)	1.7(1)
	occ	1	1	1	1
P, Si	*x*	0.4164(1)	0.4166(2)	0.4111(1)	0.4106(3)
	y	0.09448(5)	0.0946(1)	0.09593(7)	0.0958(1)
	z	¼	¼	¼	¼
	B	0.419(8)	0.79(8)	0.54(2)	1.3(1)
	occ	1	0.99(2)	0.965(4)	0.96(2)
O1	*x*	0.7402(4)	0.7403(7)	0.7234(5)	0.7222(9)
	y	0.0970(1)	0.0974(3)	0.1148(2)	0.1158(4)
	z	¼	¼	¼	¼
	B	0.73(2)	0.63(8)	1.22(4)	1.8(1)
O2	*x*	0.2062(4)	0.2056(6)	0.1712(5)	0.1671(9)
	y	0.4570(1)	0.4566(3)	0.4493(2)	0.4484(4)
	z	¼	¼	¼	¼
	B	0.65(2)	0.79(8)	1.19(4)	1.8(1)
O3	*x*	0.2836(2)	0.2841(4)	0.2678(3)	0.2666(6)
	y	0.1649(1)	0.1646(2)	0.1688(1)	0.1690(3)
	z	0.0472(2)	0.0471(3)	0.0470(3)	0.0469(4)
	B	0.69(2)	0.79(8)	1.17(3)	1.7(1)
a [Å]		4.7006(4)	4.7010(4)	4.799(3)	4.795(1)
b [Å]		10.341(1)	10.335(1)	10.037(6)	9.992(2)
c [Å]		6.0166(5)	6.0163(6)	5.918(3)	5.886(2)

*B constrained to that of natural triphylite (Trip79, 9706.41)

as analytical ones is particularly useful to reduce matrix effects affecting light-element ionization and improve the reproducibility of analysis.

We used as reference material for Li, triphylite from the Buranga pegmatite (Rwanda), with a Li content of 9.96 wt.% Li_2O (Héreng 1989, Table 1). The calibration factor for Li was obtained through the calculation of the experimental Li ion yield after choosing P and Fe as the internal reference elements for the matrix. We thus derived the ion yields for Li relative to P and to Fe, respectively, i.e., IY(Li/P) and IY(Li/Fe), where $IY(Li/P)=(Li^+/P^+)/(Li(at)/P(at))$, Li^+ and P^+ are the current intensities and (at) represents the elemental atomic concentration. A similar definition holds for IY(Li/Fe). The two ion yields were thus used to calculate the Li_2O concentrations (wt%) in the "unknown" compounds. The mean of these two independent Li_2O evaluations, and their standard deviations (1σ), are reported in Table 9. In most cases, the relative standard deviation was ≤10 % at the 1σ-level at each spot.

Characterization of starting materials

Synthetic lithiophilite, $LiMnPO_4$

The dryly synthesized lithiophilite ($LiMnPO_4$) consisted of a fine grained slightly pink powder. Optical inspection using a polarization microscope revealed a grain size below 10 μm. Phase purity was confirmed by XRPD revealing the presence of pure lithiophilite, $LiMnPO_4$ (PDF# 74–375). Using Rietveld analysis the powder diffraction pattern could be fitted to an R_{wp}-value of 16.7 % for lithiophilite (Lit-0, Table 4). The calculated lattice parameters and fractional atomic

Table 4 Structural data and lattice parameters of lithiophilite from Rietveld refinements (space group *Pbnm*)

	Site	synth. $LiMnPO_4$ (Yonemura et al. 2004)	synth. lithiophilite Lit-0 this work	lithiophilite Tri-74 this work
M1	*x*, *y*, *z*	0, 0, 0	0, 0, 0	0, 0, 0
	B	1	–	–
M2	*x*	0.9705(4)	0.9700(9)	0.971(2)
	y	0.2815(1)	0.2817(3)	0.282(6)
	z	¼	¼	¼
	B	0.6	–	–
	P *x*	0.4087(5)	0.411(1)	0.410(3)
	y	0.0928(2)	0.0916(6)	0.092(1)
	z	¼	¼	¼
	B	0.6	–	–
O1	*x*	0.7328(11)	0.724(3)	0.740(6)
	y	0.0940(6)	0.096(2)	0.092(3)
	z	¼	¼	¼
	B	1	–	–
O2	x	0.2167(9)	0.219(2)	0.205(5)
	y	0.4563(6)	0.455(2)	0.456(3)
	z	¼	¼	¼
	B	1	–	–
O3	x	0.2778(7)	0.280(2)	0.281(3)
	y	0.1623(4)	0.161(1)	0.159(2)
	z	0.052(7)	0.049(2)	0.050(3)
	B	1	–	–
a [Å]		4.7445(2)	4.7438(4))	4.7426(6)
b [Å]		10.4466(3)	10.4476(8)	10.449(1)
c [Å]		6.1033(2)	6.1037(4)	6.1024(6)
$B_{overall}$		–	0.41(6)	0.50(8)
R_p/R_{wp}		5.96/8.37	11.5/16.7	9.3/12.4
GOF/R_{exp}		1.21/6.91	1.3/12.8	1.5/8.2

Occupancy of all positions=1

coordinates fitted well with data from Yonemura et al. (2004) for their synthetic material.

Natural triphylite

The natural triphylite sample 9706.41 (Palermo Mine, N.H. USA) was a greenish single crystal with dimensions of 8×5×10 cm. In thin section the triphylite was colorless, but showed many small inclusions of opaque crystals with sizes in the submicron range. X-ray powder diffraction of several pieces did not show a significant presence of any phases other than triphylite, $LiFePO_4$ (PDF# 40–1499) (Fig. 1a). However, using backscattered electron (BSE) imaging in combination with electron microprobe measurements small lenses of sarcopside, $Fe_3(PO_4)_2$, with dimensions of 100×10 μm were identified. Recently Libowitzky et al. (2012) identified lamella of sarcopside in a gem-quality triphylite-lithiophilite from Brazil using micro-Raman spectroscopy. In order to analyze the composition of our triphylite crystal and to check its homogeneity, EPMA measurements were performed on two thin sections perpendicularly oriented to each other (Table 7). Besides P, Fe, and Mn appreciable amounts of Mg, as well as minor amounts of Na and Si were detected. The crystal was found to be homogeneous in composition and characterized by a Fe number of x_{Fe}=Fe/(Fe+Mn+Mg)=0.73 (1). Figure 2a shows a ^{57}Fe-Mössbauer spectrum of a powdered sample prepared from pieces taken from several parts of the triphylite crystal. The spectrum shows a single quadrupole doublet with Mössbauer parameters *IS*=1.21 mm/s, *QS*=2.98 mm/s typical for ferrous iron in octahedral coordination and comparable to those given by Fehr et al. (2007) for their natural samples (Table 6). Only very minor amounts of ferric iron $Fe^{3+}/Fe^{3+}+Fe^{2+}\approx 2$ % were detected.

Table 5 Comparison of unit cell parameters of $Li_{1-0}(Fe,Mn)PO_4$ phases. (setting according to space group *Pbnm*)

	Sample	*a* [Å]	*b* [Å]	*c* [Å]	*V* [Å^3]
Triphylite, $Li(Fe^{2+},Mn^{2+})PO_4$					
This work	nat., 9706.41	4.7010(4)	10.335(1)	6.0163(6)	292.30(5)
(Losey et al. 2004)	nat., Trip79	4.7006(4)	10.341(1)	6.0166(5)	292.46(4)
(Andersson et al. 2000)	syn. $LiFePO_4$	4.6908(2)	10.3290(3)	6.0065(2)	291.02(2)
Ferrisicklerite, $Li_{<1}(Fe^{3+},Mn^{2+})PO_4$					
This work	syn., Tri-77	4.795(1)	9.992(2)	5.886(2)	282.01(5)
(Alberti 1976)	nat., ferrisick.	4.799(3)	10.037(6)	5.918(3)	285.05(2)
Lithiophilite, $LiMn^{2+}PO_4$					
This work	syn., Lit-0	4.7438(4)	10.4476(8)	6.1037(4)	302.45(4)
This work	syn., Tri-74	4.7426(6)	10.446(1)	6.1024(6)	302.32(3)
(Losey et al. 2004)	nat., Trip06	4.7383(1)	10.429(1)	6.0923(4)	301.05(4)
(Yonemura et al. 2004)	syn. $LiMnPO_4$	4.7445(2)	10.4466(3)	6.1033(2)	302.50(3)
Heterosite, $\square Fe^{3+}PO_4$					
(Andersson et al. 2000)	syn. heterosite	4.7820(2)	9.8142(2)	5.7893(2)	271.70(2)
(Padhi et al. 1997)	syn. heterosite	4.788(1)	9.821(1)	5.792(1)	272.35(9)
Purpurite, $\square Mn^{3+}PO_4$					
(Li et al. 2002)	syn. $MnPO_4$	4.78	9.69	5.93	274.7

Results

Experiments with triphylite bulk material

The reaction of triphylite powder with a $KMnO_4$-containing aqueous solution as oxidant agent (Table 1) between 70 and 170 °C resulted in black lustrous grains having the same dimensions as those of the starting material. In thin section under polarized light they show an opaque rim with a thickness of around 20 μm and homogeneous red-brown absorption colors with strong pleochroism. Under crossed polarizers they extinct homogeneously and show homogeneous interference colors indicating that the reaction has proceeded throughout the grains. Qualitative phase analysis using X-ray powder diffraction (Fig. 1b) revealed that the product phase is ferrisicklerite, $Li_{1-x}(Fe^{3+},Mn^{2+})PO_4$ (PDF-29-808). EPMA data revealed, with respect to the elements listed in Table 7, no significant differences in composition compared to that of the triphylite precursor. This also includes the Fe number, which is, within errors, identical in both the educt and product phase. In contrast to runs with $KMnO_4$, runs with H_2O_2 as oxidant agent showed a diversity of reaction products (Table 1). In the low-temperature region up to 80 °C ferrisicklerite was formed, whereas between 100 and 170 °C synthetic giniite (ferric), $Fe_5(PO_4)_4(OH)_3{\cdot}2H_2O$, appeared. At the highest temperature of 200 °C barbosalite, $Fe^{2+}Fe^{3+}{}_2(PO_4)_2(OH)_2$, and tavorite, $LiFe^{3+}PO_4OH$, were identified as product phases.

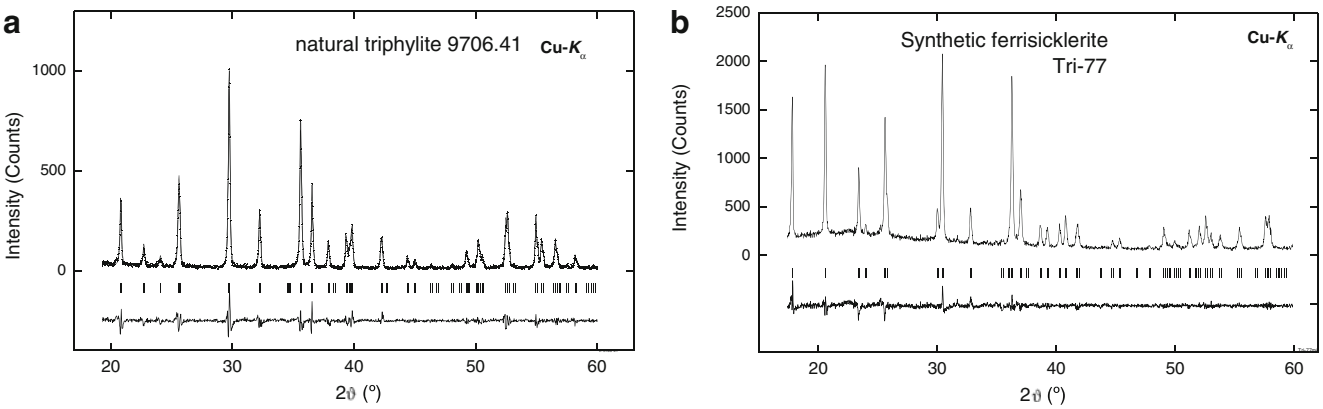

Fig. 1 **a**) and **b**) Observed, calculated and difference intensity X-ray powder diffraction patterns of natural triphylite 9706.41 and synthetic ferrisicklerite from experiment Tri-77

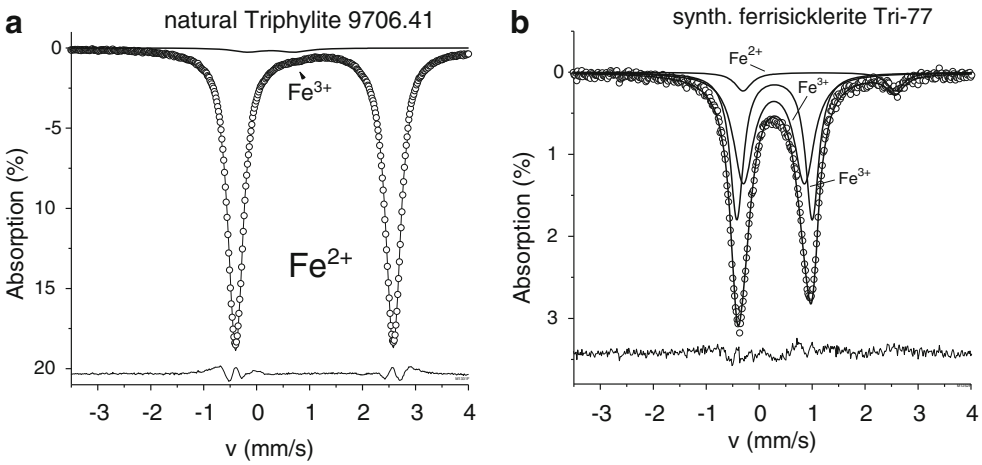

Fig. 2 **a**) and **b**) ^{57}Fe-Mössbauer spectra of natural triphylite 9706.41 starting material and synthetic ferrisicklerite from experiment Tri-77. **a**) Fit with an intense Fe^{2+} doublet and a very weak Fe^{3+} dublet. **b**) Fit with a weak Fe^{2+} doublet and two Fe^{3+} doublets. Residual are shown as lines

Single-crystal structure analysis of synthetic ferrisicklerite (Tri-77) and triphylite (9706.41)

In order to characterize the ferrisicklerite product, single-crystal structure investigations were performed. From the products of run Tri-77 (Table 1) an opaque irregular grain with a maximum diameter of 200 μm was chosen. The diffraction images showed that it consists of an intergrowth of two individual crystals, the reflections of which could be separated during indexing. Subsequently, the superimposed diffraction patterns were integrated simultaneously including an overlap control. The final choice of the domain used for the structure determination was based on the mean intensity of the data set containing the non-overlapping reflections.

Single-crystal XRD measurements of the triphylite starting material were performed using a 200 μm-sized grain that showed homogeneous extinction in polarised light. The grain was picked from the powdered material of the natural triphylite sample from Palermo Mine, N.H./USA 9706.41. Conditions of data collection and results are given in Table 2. The final full-matrix least-squares fit, based on F^2, converged to an unweighted $R1$ index of 0.0230 (triphylite) and 0.0292 (ferrisicklerite).

For both triphylite and ferrisicklerite, the Mn/Fe-ratio of the M2 position cannot be determined from X-ray diffraction data due to the similar scattering factors of both atoms. Therefore, the contribution of the M2 position was modelled according to a 100 % occupancy by Fe^{2+} in case of triphylite and by Fe^{3+} in case of ferrisicklerite neglecting the influence of minor Mg^{2+} (0.060(3) a.p.f.u., see Table 7). The M1 and P-positions were modelled with Li and P, respectively, neglecting the minute amounts of Na and Si which are assumed to be present in these sites (Table 7).

For both positions site population refinements indicated full occupancy within 1-sigma uncertainty in triphylite which is in good agreement with the chemical formula of $Li(Me^{2+})PO_4$. The results of the structure refinement of our triphylite sample can be compared to the structural data of a

Table 6 ^{57}Fe-Mössbauer parameters at room temperature of natural and synthetic triphylite and ferrisicklerite

Samples	Species	IS [mm/s]	QS [mm/s]	FWHM [mm/s]	Area [%]
Triphylite, $Li(Fe^{2+},Mn^{2+})PO_4$					
This work nat. triphylite	Fe^{2+}-M2	1.21	2.98	0.34	98
	Fe^{3+}-M2	0.27	0.88	0.66	2
(Fehr et al. 2007) nat. triphylite	Fe^{2+}-M2	1.15	2.95	0.26	100
Ferrisicklerite $Li_{<1}(Fe^{3+},Mn^{2+})PO_4$					
(Li and Shinno 1997) nat. ferrisicklerite	Fe^{3+}-M2	0.46(1)	1.04(5)	0.38(1)	56
	Fe^{3+}-M2	0.47(1)	0.75(4)	0.26(3)	27
	Fe^{2+}-M2	1.21(1)	2.92(2)	0.35(2)	17
(Liu et al. 2005) nat. ferrisicklerite	Fe^{3+}-M2	0.45	0.90	0.28	85
	Fe^{2+}-M2	1.23	2.94	0.20	15
This work syn. Ferrisicklerite, Tri-77	Fe^{3+}-M2	0.42	1.43	0.30	44
	Fe^{3+}-M2	0.41	1.16	0.44	49
	Fe^{2+}-M2	1.26	2.87	0.38	7

IS isomer shift relative to α-iron, *QS* quadrupole splitting, *FWHM* full width at half maximum

Table 7 Chemical compositions in wt % (oxides; upper half) and apfu. (cations; lower half) from EPMA.

	Triphylite 9706.41 *N*=44	Sarcopside lamella 9706.41 *N*=6	Synth. ferrisicklerite grains Tri-77 *N*=15	Opaque crust cube Tri-87 *N*=4
P_2O_5	46.1(9)	42(1)	44.9(9)	0.06(7)
SiO_2	0.26(4)	0.24(2)	0.24(2)	n.m.
FeO tot	35.1(6)	48(1)	35.9(6)	0.4(2)
Fe_2O_3 **	[0.77(1)]		[36.7(7)]	
FeO **	[34.4(6)]		[2.87(5)]	
MgO	1.54(7)	1.3(2)	1.61(7)	0.4(4)
MnO	9.9(3)	10.5(4)	11.1(4)	71(1)
ZnO	n.d.	n.d.	n.d.	0.008(20)
CaO	n.d.	n.d.	n.d.	0.11(8)
Na_2O	0.040(3)	n.d.	n.d.	0.7(5)
K_2O	n.d.	n.d.	0.11(7)	10(2)
sum	93(1)	102(2)	94(1)	83(2)
cation #	$(P,Si)O_4$	8 oxygens	$(P,Si)O_4$	
P^{5+}	0.99(2)	2.03(6)	0.99(2)	
Si^{4+}	0.007(1)	0.013(1)	0.006(1)	
Fe^{3+} **	0.015(2)	–	0.73(1)	
Fe^{2+} **	0.73(1)	2.28(5)	0.055(1)	
Mg^{2+}	0.059(3)	0.11(1)	0.063(3)	
Mn^{2+}	0.215(6)	0.50(2)	0.246(9)	
Na^{+}	0.002(1)	n.d.	n.d.	
K^{+}	n.d.	n.d.	0.004(4)	
sum	2.02(3)	4.94(8)	2.09(3)	
x_{Fe}	0.73(1)	0.79(2)	0.72(1)	

N number of averaged analyses, () standard deviation 1σ, *n.d.* not detected, *n.m.* not measured. **$Fe^{2+}/(Fe^{2+}+Fe^{3+})$=0.07 for ferrisicklerite and 0.98 for triphylite determined by Mössbauer spectroscopy (see Table 6). []: not included in the sum of oxides. X_{Fe}=Fe/(Fe+Mn+Mg)

Table 8 Chemical compositions from EPMA and SIMS data on the oxidized sample cuboid Tri-87

Triphylite Tri-87 inner cube *N*=17				Ferrisicklerite Tri-87 rim *N*=18			
	weight %		apfu. 4 O^{2-}		weight %		apfu. 4 O^{2-}
P_2O_5	45.3(7)	P^{5+}	1.00(2)	P_2O_5	46(1)	P^{5+}	1.01(3)
SiO_2	0.27(3)	Si^{4+}	0.007(1)	SiO_2	0.25(2)	Si^{4+}	0.006(1)
TiO_2	n.d.	Ti^{4+}	n.d.	TiO_2	n.d.	Ti^{4+}	n.d.
Al_2O_3	n.d.	Al^{3+}	n.d.	Al_2O_3	n.d.	Al^{3+}	n.d.
Cr_2O_3	n.d.	Cr^{3+}	n.d.	Cr_2O_3	n.d.	Cr^{3+}	n.d.
Fe_2O_3 **	0.76(1)	Fe^{3+} **	0.015(1)	Fe_2O_3 **	35.8(7)	Fe^{3+} **	0.65(1)
FeO **	33.7(3)	Fe^{2+} **	0.733(6)	FeO **	2.42(4)	Fe^{2+} **	0.049(1)
MgO	1.62(5)	Mg^{2+}	0.063(2)	MgO	1.60(5)	Mg^{2+}	0.062(2)
MnO	9.5(2)	Mn^{2+}	0.210(4)	MnO	9.8(2)	Mn^{2+}	0.218(5)
ZnO	n.d.	Zn^{2+}	n.d.	ZnO	n.d.	Zn^{2+}	n.d.
CaO	n.d.	Ca^{2+}	n.d.	CaO	n.d.	Ca^{2+}	n.d.
Li_2O^*	8.9(3)	Li^{+*}	0.93(1)	Li_2O^*	2.9(6)	Li^{+*}	0.30(7)
Na_2O	0.05(5)	Na^{+}	0.002(2)	Na_2O	0.1(1)	Na^{+}	0.006(5)
K_2O	0.02(2)	K^{+}	0.001(1)	K_2O	0.3(3)	K^{+}	0.01(1)
F	n.d.	F^{-}	n.d.	F	n.d.	F^{-}	n.d.
Sum	100.1(9)	*sum*	2.96(4)	*sum*	99(2)	*sum*	2.32(8)
		x_{Fe}	0.733(8)			x_{Fe}	0.71(2)

N number of averaged analyses, () standard deviation 1σ, *n.d* not detected, x_{Fe}: *Fe/Fe+Mn+Mg* *: SIMS data; **$Fe^{2+}/(Fe^{2+}+Fe^{3+})$=0.07 for ferrisicklerite and 0.98 for triphylite determined by Mössbauer spectroscopy (see Table 6)

Table 9 SIMS data for Li with 1σ uncertainty obtained at different transects M, AE and G of Fig. 4 over the triphylite – ferrisicklerite reaction boundary

Profile Spot	Distance[a] [μm]	Li_2O wt %	1σ Li_2O wt %	1σ Li_2O rel %
M				
M-01	66.25	3.03	0.05	1.6
M-03	36.25	2.54	0.12	4.5
M-04	16.25	2.73	0.19	7.0
M-05[b]	0	4.30	0.29	6.8
M-06	−16.25	8.80	0.15	1.6
M-07	−31.25	8.75	0.13	1.5
M-08	−48.75	9.12	0.16	1.8
M-09	−65	8.17	0.04	0.5
M-10	−78.75	9.20	0.04	0.5
A-E				
AE-02	140	3.82	0.56	15
AE-03	122.5	2.93	0.23	7.7
AE-04	107.5	2.21	0.04	2.0
AE-05	90	2.26	0.08	3.4
AE-06	72.5	2.17	0.1	4.7
AE-07	60	2.46	0.24	10
AE-08	40	2.34	0.35	15
AE-09	22.5	4.53	0.03	0.6
AE-10	3.75	3.16	0.54	17
AE-11	−10	8.58	0.21	2.5
AE-12	−22.5	8.82	0.01	0.1
AE-13	−35	9.13	0.07	0.8
AE-14	−51.25	9.36	0.08	0.9
AE-15	−65	8.47	0.16	1.9
G				
G-01	−137.5	8.64	1.03	12
G-02	−122.5	9.13	0.95	10
G-03	−106.25	8.88	0.09	1.0
G-04	−88.75	8.81	0.01	0.1
G-05	−72.5	9.26	0.26	2.8
G-06	−58.75	8.65	0.52	6.1
G-07	−38.75	8.79	1.29	15
G-08	−20	7.74	0.91	12
G −10[c]	−1.0	3.59	0.13	3.5
G −11	17.5	3.38	0.06	1.7
G −12	32.5	2.98	0.15	4.9
G −13	47.5	2.63	0.18	7.0
G −14	67.5	2.76	0.20	7.3
G −15	82.5	2.39	0.40	17
G −16	100	3.04	0.31	10

[a] The distance is measured from the reaction front

[b] at the reaction front; [C] close to the reaction front

natural triphylite (Trip79) with a similar composition given by Losey et al. (2004). The fractional atomic coordinates and the lattice parameters are identical within the limits of the uncertainties with the exception of the *b* axis parameter which is only slightly larger.

In the case of ferrisicklerite, the values of the fractional atomic coordinates (Table 3) compare well with those published by Alberti (1976). If the occupancy and the anisotropic displacement factors of the M1(Li)-position are varied independently, the occupancy converges to a value of 58(8)% and the equivalent displacement factor resulted in B_{eq}=4.7 Å^2. The latter is approximately six times higher than that of the fully occupied M1-Li position in triphylite (B_{eq}=0.78 Å^2). Because of the generally strong correlation between the occupancy and the displacement factor and the fact that lithium is a very weak scatterer for X-rays, the Li-position in ferrisicklerite was further modelled with an isotropic temperature factor B_{iso} that was fixed to the value of the B_{eq} refined for the M1 (Li)-position in triphylite (B_{eq}=0.78 Å^2). Using this procedure, the occupancy of the M1-Li position finally converged at a value of 32(2)%.

Rietveld analysis of synthetic ferrisicklerite

In order to characterize the bulk phase composition, the powder diffraction pattern of our synthetic ferrisicklerite Tri-77 was analyzed by the Rietveld method using the lattice parameters and structural data of our single-crystal investigation (Table 3) as starting parameters. Only lattice parameters and an overall isotropic displacement parameter $B_{overall}$ were refined. The results are given in Fig. 1b. The data could be refined to a R_{wp} value of 11.9 %. All the detected diffraction lines could be assigned to ferrisicklerite and therefore no other phases were detected. Compared to the powder diffraction data of natural triphylite (Fig. 1a), the diffraction pattern of ferrisicklerite showed significantly higher background intensity in the range between 20 and 30° 2Θ which indicates the presence of a X-ray amorphous phase.

^{57}Fe-Mössbauer spectroscopy

The ^{57}Fe-Mössbauer spectrum of the synthetic ferrisicklerite sample Tri-77 (Fig. 2b) consists of two dominating absorption lines at≈−0.4 mm/s and≈1 mm/s and one weaker line at≈2.5 mm/s. The stronger lines were fitted using two quadrupole doublets (Table 6) with isomer shifts of *IS*= 0.42 and 0.41 mm/s and quadrupole splittings of *QS*=1.16 and 1.43 mm/s typical for ferric iron in octahedral coordination. The weaker ones were fitted using one quadrupole doublet with an isomer shift of *IS*=1.26 mm/s and a quadrupole splitting of *QS*=2.87 mm/s that was assigned to octahedrally coordinated ferrous iron (Fehr et al. 2007; Liu

et al. 2005; Li and Shinno 1997). Therefore, approximately 93 % of the total iron in our synthetic ferrisicklerite sample (Tri-77) is in the ferric oxidation state and only a small amount of ferrous iron is left.

Experiment using a cuboid of natural triphylite as educt

The results of our oxidation experiment with a cuboid cut from a natural triphylite crystal are given in Table 1. After having treated the cuboid for 8 days in a 0.1 N HCl solution at 120 °C the formerly greenish triphylite cuboid has developed a lustrous black crust (Fig. 3). Inspection under polarized light in thin section showed that two new layers have formed. The outermost part is composed of an opaque brittle layer with a thickness of around 20 μm followed by an intensively colored red-brown layer with a varying thickness between 50 and 100 μm. The latter layer showed strong pleochroism and was found in direct contact to the inner unreacted triphylite (Fig. 4). Between the latter two phases an irregularly shaped, but often sharp boundary has formed that was often but not generally oriented along inner cracks. Using polarizing microscopy the red–brown reaction rim showed the same extinction angles as the unreacted triphylite inner core. Figs. 4a) and b) show backscattered electron images of the educt (triphylite) and product (ferrisicklerite) along the phase boundary. Ferrisicklerite can be recognized by a slightly brighter shade of grey compared to the inner unreacted triphylite. Ferrisicklerite shows a rougher surface with pores in the submicron range compared to the inner triphylite.

In total three chemical profiles were measured across the triphylite – ferrisicklerite reaction boundary by EPMA and SIMS (Fig. 4a and b). The elements P, Fe, Mn, Mg, K, and Si were measured by EPMA, whereas the Li content was determined by SIMS (Table 9 and Fig. 5). The mean values of the compositional data for the two phases are given in Table 8. Combining the EPMA, SIMS and Mössbauer data (Table 8) the composition of the triphylite sample was found to be $Li_{0.93(3)}(Fe^{2+}_{0.733(6)},Fe^{3+}_{0.015(1)},Mn^{2+}_{0.210(4)},Mg_{0.063(2)})_{1.021(8)}P_{1.00(2)}O_4$ and that of our synthetic ferrisicklerite was calculated to be $Li_{0.30(7)}(Fe^{3+}_{0.65(2)}Fe^{2+}_{0.049(1)}Mn_{0.218(5)}Mg_{0.062(2)})P_{1.01(3)}O_4$.

Fig. 3 Thin section of the triphylite cuboid sample after the oxidation run. The small sections in the white rectangles are shown as BSE images in Fig 4 a and b, respectively

Experiments with dryly synthesized lithiophilite bulk material

An experiment (Tri-74) with synthetic lithiophilite, $LiMnPO_4$ as educt was performed under the same conditions as those with the cuboid and powdered material of the natural triphylite (Table 1). After the run no changes in phase composition (Table 1) and lattice parameters were detected. The results of the Rietveld refinement of the lithiophilite from Tri-74 are presented together with literature data in Table 4. The powder diffraction could be fitted to an R_{wp}-value of 12.4 %, and the uncertainties of the fractional atomic coordinates for our lithiophilite are comparable to those given by Yonemura et al. (2004).

Discussion

In this paper we focus on the experimental reconstruction of the topotactic oxidation reaction of triphylite-lithiophilite solid solutions to the Li-depleted solid solutions ferrisicklerite-sicklerite. In a special oxidation experiment starting with a polished triphylite cuboid of natural triphylite we have shown that at a temperature of 120 °C it is possible to mimic the reaction texture found in nature. The reaction triphylite =>ferrisicklerite forms an irregular rim with an average thickness of about 100 μm (Fig. 3). This rim consists of two layers (Fig. 4). The outermost layer is rich in potassium and manganese and is interpreted as a precipitate of the reduced $KMnO_4$ which was used as oxidant agent. The second layer consists of ferrisicklerite showing the typical red-brown absorption colors and a strong pleochroism as it was reported for ferrisicklerite replacing triphylite in nature (Fransolet et al. 1986). Between these layers a small gap marks the original surface of the triphylite cuboid. This observation has also been made in other experimental studies that investigated fluid-mediated replacement reactions (e.g., Pöml et al. 2007; Geisler et al. 2010). The experimentally formed boundaries between ferrisicklerite and triphylite are often sharp on the micrometer-scale or even below (Fig. 4) as was also reported for natural associations (Fontan et al. 1976; Fransolet et al. 1986). Situations, where there is an apparent continuous change from red-brown ferrisicklerite to triphylite, can be explained by an

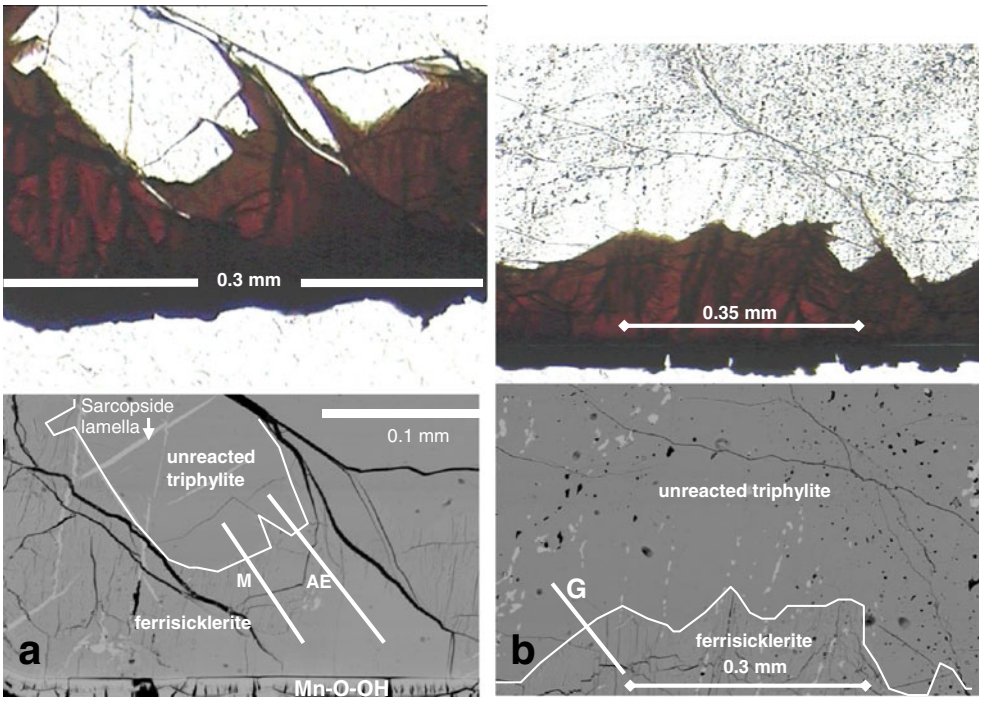

Fig. 4 **a**) and **b**) BSE (*down*) and transmitted light optical micrographs (*up*) within the rectangular areas **a** and **b** of Fig. 3 with the transects M, AE and G (*bold white line*) and reaction front between triphylite and ferrisicklerite (*thin white line*). A grey sarcopside exsolution lamella is revealed in BSE contrast (**a**)

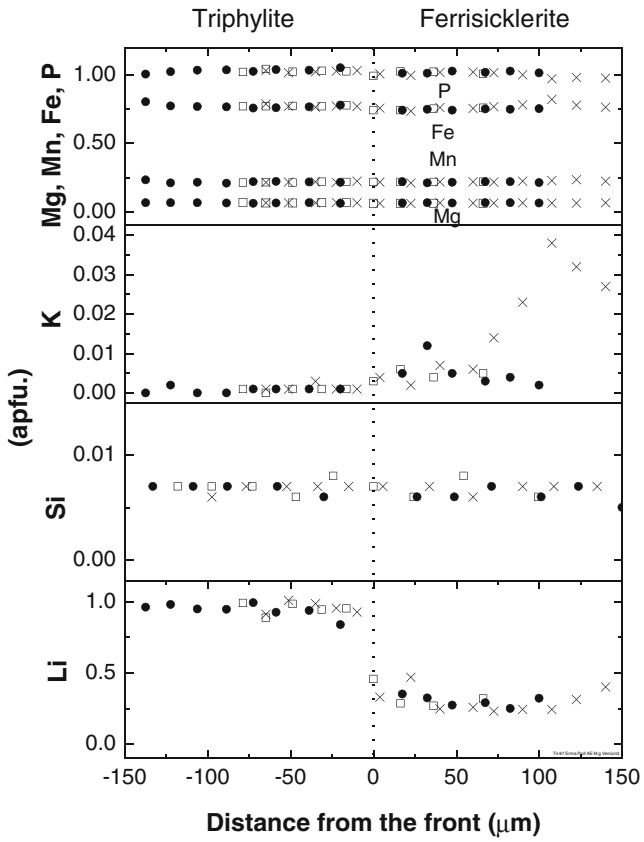

Fig. 5 Chemical composition in atoms per formula unit (apfu.) using $(Li,K)(Fe,Mn,Mg)(P,Si)O_4$ along the three transects AE (cross), M (*open square*) and G (*full circle*) across the reaction front starting from unreacted triphylite to the product phase ferrisicklerite. (Sample Tri-87). Li: SIMS data; Si, K, Mn, Mg, P and Fe: EPMA data

inclined orientation of the reaction front relative to the surface of the thin section.

It is noteworthy to mention that Hatert et al. (2012) observed a progressive transition from lithiophilite to sicklerite in samples from the Altai Mountains, China. This transition is visible under the polarizing microscope (Fig. 1 in Hatert et al. 2012), and corresponds to a progressive change in composition, evolving from $Li_{0.93}(Mn^{2+}_{0.80}Fe^{3+}_{0.13}Fe^{2+}_{0.04})PO_4$ (lithiophilite) to $Li_{0.69}(Mn^{2+}_{0.62}Mn^{3+}_{0.19}Fe^{3+}_{0.16})PO_4$ (sicklerite). The situation occurring in the lithiophilite-sicklerite series is consequently different from that occurring in the triphylite-ferrisicklerite series, certainly due to the different oxidation behaviors of iron and manganese.

Oxidation state of iron and manganese

One striking feature of the Mason-Quensel sequence is the progressive oxidation of the cations Fe^{2+} and Mn^{2+}. Due to the higher oxidation potential of divalent manganese ferrous ion is first oxidized. The ^{57}Fe-Mössbauer spectrum of our ferrisicklerite (Tri-77) shows that the major part of iron is in the ferric state (~ 93 %) in agreement with the general formula of ferrisicklerite $Li_{<1}(Fe^{3+},Mn^{2+})PO_4$ (Table 6). By comparison with the natural triphylite starting material, containing only Fe^{2+}, it is evident that most of the ferrous iron has been transformed to the ferric state. The remaining 7 % of ferrous iron could be incorporated into the ferrisicklerite, but it is also possible that it is bound to minute amounts of unreacted triphylite or to passive inclusions, such as, e.g., the sarcopside lamella (Fig. 4).

^{57}Mössbauer spectra of ferrisicklerite-sicklerite were reported by Liu et al. (2005) and Li and Shinno (1997). They are very similar to our spectrum and also characterized by two intense absorptions near~−0.1 mm/s and ~0.8 mm/s and a weak one at ~2.8 mm/s. They were fitted by the authors with subspectra for ferric and ferrous iron (Table 6). The two intense absorptions were mainly attributed to Fe^{3+} placed in the M2 octahedra of the olivine type structure, but modelled in different ways by the two groups of authors. Li and Shinno (1997) fitted their ferrisicklerite spectrum using two doublets with isomer shifts of about ~0.46–0.47 mm/s, whereas Liu et al. (2005) used one Voigt-based quadrupole splitting distribution (QSD) for the Fe^{3+} with a relatively broad Gaussian distribution. Both groups interpreted the line broadening as reflecting next nearest neighbor (NNN) effects, originating from the distribution of iron and manganese ions over neighboring M2 positions as well as from the distribution of the Li^+ ions over the incompletely occupied M1 positions. Both groups reported for the Fe^{3+}-M2 position a smaller quadrupole splitting of QS=0.75–1.04 and 0.90 mm/s when compared to our results of QS=1.16–1.43 mm/s (Table 6). This may be due to the fact that their ferrisicklerite was rich in manganese with x_{Fe}=0.14 (and should be named sicklerite rather than ferrisicklerite), whereas the ferrisicklerite in this study is rich in Fe with x_{Fe}=0.72(1) (Table 7).

Based on the SIMS, EPMA and ^{57}Fe-Mössbauer results for the synthetic ferrisicklerite we calculated the charge-balanced formula $Li_{0.30(7)}(Fe^{2+}_{0.049(1)}Fe^{3+}_{0.65(2)}Mn^{2+}_{0.218(5)}Mg_{0.062(2)})_{0.98(1)}P_{1.01(3)}O_4$. In contrast to the ferrisicklerite studied by Liu et al. (2005), and Li and Shinno (1997), it was not necessary to assume the presence of trivalent manganese. Moreover, the absence of Mn^{3+} in our synthetic ferrisicklerite is supported by our experiment with synthetic lithiophilite, $LiMnPO_4$ (Sample Tri-74 from Table 1) as starting material. As can be seen from Table 4, neither the lattice parameters nor the fractional atomic coordinated of $LiMnPO_4$ differ significantly before and after the run. This means that the oxidant agent $KMnO_4$ was not able to oxidize manganese to the trivalent state. Therefore we conclude that in our synthetic ferrisicklerite manganese is only present in the divalent state.

Chemical profiles: the role of potassium to stabilize ferrisicklerite

Using EPMA we have measured chemical profiles across the reaction front (Fig. 5). The main elements P, Fe, Mn, Mg, as well as Si do not show significant variations in their concentrations across the reaction interface. This seems to be a typical chemical feature of this reaction as the same observation was reported for associated triphylite and ferrisicklerite from the Tsaobismund pegmatite (Fransolet et al. 1986). However, an exception is the increase of the potassium content in the ferrisicklerite rim starting at the reaction front (Fig. 5). In triphylite the potassium content was found to be 0.02(2) wt%, which is close to the detection limit of our EPMA measurements. This is reasonable because with an ionic radius of 1.38 Å (Shannon 1976) the potassium ion seems to be too large to replace Li^+ (r=0.76 Å) in octahedral coordination in significant amounts. Nevertheless in ferrisicklerite the detected amount of potassium was found to increase systematically with the distance from the reaction front (Fig. 5). As the same structural arguments concerning substitution of Li^+ by K^+ ions in triphylite also hold for ferrisicklerite, it seems to be unlikely that the detected potassium ions are incorporated into the structure of ferrisicklerite. A first hint to the solution of this problem comes from the inspection of the BSE images in Fig. 4a) and b) which shows the same area as the polarizing microscope images in the same figure. By comparing the surface structure of the inner pristine triphylite with that of the product ferrisicklerite, it can be seen that the surface of the latter appears to be significantly coarser. This appearance of the surface can be interpreted as the result of porosity which developed during the reaction process. Such porosity might be interpreted as a result of a coupled dissolution-reprecipitation process in the sense of Putnis (2002), and is often observed when the molar volume and solubility of the reaction product is smaller than that of the parent phase. The volume of the unit cell of ferrisicklerite ($V_{unit\ cell}$=282.01(4) Å^3) is smaller than that of the triphylite ($V_{unit\ cell}$=292.77(9) Å^3) (Table 5), i.e., the reaction involves a volume deficit of about 3.7 %. Therefore the single spots with high potassium content in ferrisicklerite measured with EPMA can be interpreted as to be due to a potassium compound precipitated from the reacting aqueous solution present in the pores.

A second explanation for this K increase in ferrisicklerite is based on the structural features of these olivine-type phosphates. In the lithiophilite-sicklerite series, Hatert et al. (2012) showed a negative correlation between the M1-O and M2-O bond distances, which is due to crystal-chemical constraints. Indeed, the olivine structure is extremely compact, and each oxygen is bound to both *M*1 and *M*2 sites, thus explaining why a volume increase of one of these sites implies a volume decrease of the adjacent crystallographic site. The oxidation of iron in ferrisicklerite certainly produces a decrease of the M2-O bond lengths, compensated by a significant increase of the M1-O bond lengths. These longer bonds could explain the presence of small amounts of larger cations on that site, as for example K, as observed in our experiments.

An increase of trace elements in ferrisicklerite and heterosite, compared to parent triphylite, was already described in the literature. Baijot et al. (2009, 2012) observed an increase of the K and Ca contents in ferrisicklerite and heterosite from the Sapucaia pegmatite, Brazil, in which the K_2O contents reach 0.45 wt.% which is in the same order of magnitude as

the K_2O contents of 0.11(7) wt. % and 0.3(3) wt. % measured in our experiments (Tables 7 and 8). Fransolet et al. (1986) also observed an increase of the Ca contents in ferrisicklerite and heterosite from the Tsaobismund pegmatite, in which up to 0.21 wt.% CaO was detected. These authors underline the role of these trace elements in stabilizing the crystal structures of ferrisicklerite and heterosite.

Although K concentrations increase at the reaction front, the reaction front is chemically better defined by the Li^+ composition profile (Fig. 5). On sample Tri-87 we have measured three profiles by SIMS that were located close to the electron microprobe spots (Fig. 4a and b). In Fig. 5 the data of all three profiles are plotted versus the distance of the measured spot from the reaction front. The Li^+ content drops at the reaction front within a length scale of 15 μm from approximately one atom per formula unit (~ 1 apfu) in triphylite to 0.30(7) apfu. in ferrisicklerite. The Li^+ content in ferrisicklerite was also confirmed by single-crystal X-ray diffraction (Li occupancy of 0.32(2)). The agreement of the experimental data from both independent analytical techniques is within 1σ error.

Influence of the oxidation potential

Runs with the same triphylite starting material, but different oxidant agents $KMnO_4$ and H_2O_2, led to different reaction products (Table 1). Using $KMnO_4$ and temperatures between 70 and 170 °C replacement of triphylite by ferrisicklerite was observed. In contrast, using 30 % H_2O_2 (aq) ferrisicklerite formed as a product only in the temperature range between 60 and 80 °C. At higher temperatures of 100 to 170 °C ferric giniite $Fe^{3+}{}_5(PO_4)_4(OH)_3 \cdot 2H_2O$, and at 200 °C a mixture of barbosalite, $Fe^{2+}Fe^{3+}{}_2(PO_4)_2(OH)_2$, together with tavorite, $LiFe^{3+}PO_4(OH)$, was identified as replacement products (Table 1).

Whereas the mineral giniite contains both ferrous and ferric iron, the giniite phase identified in our experiments corresponds to an isotypic, but synthetic compound that contains only ferric iron. Ferric giniite is known as an alteration product in pegmatitic rocks (Song et al. 2002; Ann et al. 2000). Experimentally, it forms from amorphous Fe phosphate precursors at temperatures above 150 °C (Roncal-Herrero et al. 2009). Barbosalite and tavorite are known as secondary minerals from granitic pegmatites. Fransolet et al. (1986) have identified both minerals as alteration products replacing triphylite in the Tsaobismund pegmatite. According to mentioned authors, tavorite and barbosalite formed from "triphylite 1" under low-temperature hydrothermal conditions. According to our results $KMnO_4$ favors the formation of ferrisicklerite from triphylite when compared to H_2O_2 which favors the formation of ferric giniite or tavorite and barbosalite. This result shows that the reaction product depends on the redox potential of the surrounding fluid. This has to be taken into account when characterizing the conditions of mineral formation in pegmatites, even when fully oxidized phases were formed.

Conclusions

We have shown that under hydrothermal conditions in the temperature range between 60 and 170 °C triphylite, $Li(Fe^{2+},Mn^{2+})PO_4$ can be oxidized to form ferrisicklerite, $Li_{<1}(Fe^{3+},Mn^{2+})PO_4$. Therefore, the first reaction step of the Mason-Quensel sequence can be reconstructed experimentally, using $KMnO_4$ or H_2O_2 as oxidant agents.

It was found that this reaction was dependent on the oxidation potential, as the use of less oxidizing H_2O_2 led at higher temperatures to the formation of other phases such as barbosalite, ferric giniite, and tavorite compared to the stronger oxidant agent $KMnO_4$. Moreover, the presence of significant amounts of K in synthetic ferrisicklerite indicates that small amounts of trace elements such as Ca or K may have a stabilizing influence on the crystal structure of ferrisicklerite and heterosite if these elements are incorporated into the structure of these minerals. At 120 °C the textures of the topotactic reaction triphylite⇒ferrisicklerite resemble those found in natural samples. The product ferrisicklerite was found to grow epitactical on the educt triphylite, proving the topotactical character of this reaction.

In conclusion, the oxidation of triphylite to ferrisicklerite requires: (i) a temperature below 200 °C, since high temperature experiments produce phases such as tavorite or $Li_3Fe_2(PO_4)_3$ (Schmid-Beurmann et al. 2004; Schmid-Beurmann and Hatert 2005); (ii) a high oxidation potential, necessary to oxidize Fe^{2+} to Fe^{3+}; and (iii) the presence of small amounts of K or Ca, which seems to play a significant role in stabilizing the crystal structure of ferrisicklerite at higher temperatures than 80 °C. Our experimental results demonstrate that the existence of primary ferrisicklerite in granitic pegmatites, suggested by Roda et al. (1996); Roda Robles et al. (1998); Roda et al. (2004) could be better interpreted as an oxidation and replacement product of triphylite, formed under low-temperature and highly oxidizing hydrothermal conditions.

Acknowledgments We thank Paul Keller (Stuttgart) who provided the triphylite single crystal from Palermo Mine, New Hampshire, USA.

References

Alberti A (1976) Crystal structure of ferrisicklerite, $Li_{<1}(Fe^{3+}, Mn^{2+})PO_4$, locality: Sidi-Bou-Othmane, Jebilet, Morocco. Acta Crystallogr B32:2761–2764

Altomare A, Cascarano G, Giacovazzo A, Burla MC, Polidori G, Carmalli M (1992) SIR92 – a program for automatic solution of structures by direct methods. J Appl Crystallogr 27:435–436

Andersson AS, Kalska B, Häggström L, Thomas JO (2000) Lithium extraction/insertion in $LiFePO_4$: an X-ray diffraction and Mössbauer spectroscopic study. Solid State Ionics 130:41–52

Ann Y, Reddy KR, Delfino JJ (2000) Influence of redox potential on phosphorus solubility in chemically amended wetland organic soils. Ecol Eng 14:169–180

Baijot M, Hatert F, Philippo S, Cassedane J, Fransolet A-M (2009) Mineralogy and petrography of phosphate minerals from Sapucaia and Boca Rica pegmatites, Minas Gerais, Brazil. Estudos Geol-Madrid 19:47–51

Baijot M, Hatert F, Philippo S (2012) Mineralogy and geochemistry of phosphates and silicates in the Sapucaia pegmatite, Minas Gerais, Brazil: genetical implications. Can Mineral, in press

Bjoerling C, Westgren A (1938) Minerals of the Varutrask pegmatite. IX. X-ray studies on triphylite, varulite, and their oxidation products. Geol Foren Stock For 60:67–72

Eventoff W, Martin R, Peacor DR (1972) The crystal structure of heterosite. Am Mineral 57:45–51

Fehr KT, Hochleitner R, Schmid-Bauer R, Schneider J (2007) Mineralogy, Mössbauer spectra and electrical conductivity of triphylite Li(Fe2+, Mn2+)PO4. Phys Chem Miner 34:485–494

Finger LW, Rapp GR (1969) Refinement of the crystal structure of triphylite. Carnegie I Wash 68:290–292

Fontan F, Huvelin P, Orliac M, Permingeat F (1976) La ferrisicklerite des pegmatites des Sidi-bou-Othmane (Jelibet, Maroc) et le groupe des minéraux á structure de triphylite. B Soc Fr Mineral Cr 99:274–286

Fransolet A-M, Keller P, Fontan F (1986) The phosphate mineral associations of the Tsaobismund pegmatite, Namibia. Contrib Mineral Petr 92:502–517

Fransolet A-M, Hatert F, Fontan F (2004) Petrographic evidence for primary hagendorfite in an unusual assemblage of phosphate minerals, Kibingo granitic pegmatite, Rwanda. Can Mineral 42:697–704

Geisler T, Janssen A, Scheiter D, Stephan T, Berndt J, Putnis A (2010) Aqueous corrosion of borosilicate glass under acidic conditions: a new corrosion mechanism. J Non-Cryst Solids 356:1458–1465

Hatert F, Fransolet A-M, Maresch W (2006) The stability of primary alluaudite in granitic pegmatites: an experimental investigation of the $Na_2(Mn_{2-2x}Fe_{1+2x})(PO_4)$ system. Contrib Mineral Petr 152:399–419

Hatert F, Ottolini L, Schmid-Beurmann P (2011) Experimental investigation of the alluaudite+triphlyite assemblage, and development of the Na-in-triphylite geothermometer: application to natural pegmatite phosphates. Contrib Mineral Petr 161:531–546

Hatert F, Ottolini L, Wouters J, Fontan F (2012) A structural study of the lithiophilite-sicklerite series. Can Mineral 50:843–854

Héreng P (1989) Contribution á l´étude minéralogique de phosphate de fer et de manganese de la pegmatite de Buranga, Rwanda. Master thesis, Université de Liège, p. 101

Hovestreydt E (1983) On the atomic scattering factor of O^{2-}. Acta Crystallogr A39:268–269

Ibers JA, Hamilton WC (eds) (1974) International tables for X-ray crystallography, vol IV. The Kynoch Press, Birmingham

Keller P, von Knorring O (1989) Pegmatites at the Okatimukuju farm, Karibib, Namibia, part I: phosphate mineral associations of the Clementine II pegmatite. Eur J Mineral 1:567–593

Li Z, Shinno I (1997) Next nearest neighbour effects in triphylites and related phosphate minerals. Mineral J 19:99–107

Li GH, Azuma H, Tohda M (2002) $LiMnPO_4$ as the cathode for lithium batteries. Electrochem Solid St 5:A135–A137

Libowitzky E, Beran A, Wieczorek AK, Wirth R (2012) On the presence of a hydrous component in a gemstone variety of intermediate olivine-type triphylite-lithiophilite, Li(Fe, Mn)PO4. Mineral Petrol 105:31–39

Liu Z, Dong D, Liu M, Sui Y, Su W, Qiun Z, Li Z (2005) Quadrupole splitting distributions in purpurite and related minerals. Hyperfine Interact 163:13–27

Losey A, Rakovan J, Hughes JM (2004) Structural variation in the lithiophilite-triphylite series and other olivine-group structures. Can Mineral 42:1105–1115

Mason B (1941) Minerals of the Varuträsk pegmatite. XXVIII. Some iron-manganese phosphate minerals and their alteration products, with special reference to material from Varuträsk. Geol Foren Stock For 63:117–175

Moore PB (1971) Crystal chemistry of the alluaudite structure type: contribution to the paragenesis of pegmatite phosphate giant crystals. Am Mineral 56:1955–1975

Ottolini L, Bottazzi P, Vanucci R (1993) Quantification of lithium, beryllium and boron in silicates by secondary ion mass spectrometry using conventional energy filtering. Anal Chem 65:1960–1968

Ottolini L, Camara F, Hawthorne FC, Stirling J (2002) SIMS matrix effects in the analysis of light elements in silicate minerals: comparison with SREF and EPMA data. Am Mineral 87:1477–1485

Padhi AK, Nanjundaswamy KS, Goodenough JB (1997) Phospho-olivines as positive-electrode materials for rechargeable lithium batteries. J Electroch Soc 144:1188–1194

Pöml P, Menneken M, Stephan T, Niedermeier D, Geisler T, Putnis A (2007) Mechanism of hydrothermal alteration of natural self-irradiated and synthetic titanate-based pyrochlore. Geochim Cosmochim Ac 71:3311–3322

Putnis A (2002) Mineral replacement reactions: from macroscopic observations to microscopic mechanisms. Min Mag 66:689–708

Quensel P (1937) Minerals of the Varuträsk pegmatite. I. The lithium-manganese phosphate –minerals. Geol Foren Stock For 59:77–96

Roda Robles E, Fontan F, Pesquera Pérez A, Keller P (1998) The Fe-Mn phosphate associations from the Pinilla de Fermoselle pegmatite, Zamora, Spain: occurrence of kryzhanovskite and natrodufrénite. Eur J Mineral 10:155–167

Roda E, Fontan F, Pesquera A, Velasco F (1996) The phosphate mineral association of the granitic pegmatites of the Fregeneda area (Salamanca, Spain). Min Mag 60:767–778

Roda E, Pesquera A, Fontan F, Keller P (2004) Phosphate mineral associations in the cañada pegmatite (Salamanca, Spain): paragenetic relationships, chemical compositions, and implications for pegmatite evolution. Am Mineral 89:110–125

Rodriguez-Carvajal J (2005) Full Prof Suite2005. Lab. de Léon Brillouin (CEA-CNRS). CEA/Saclay, France

Roncal-Herrero T, Rodriguez-Blanco JD, Benning LG, Oelkers EH (2009) Precipitation of iron and aluminum phosphates directly from aqueous solution as a function of temperature from 50 to 200 °C. Cryst Growth Des 9:5197–5205

Schmid-Beurmann P, Hatert F (2005) Experimental Fe^{2+}-oxidation in triphylite, $LiFePO_4$: possible formation of ferrisicklerite and heterosite. Ber Deut Min Ges, Bei Eur J Mineral 17:118

Schmid-Beurmann P, Moavenian M, Hatert F (2004) Phase stability of triphylite, $LiFePO_4$, and the phases of the Mason-Quensel-sequence. Ber Deut Min Ges, Bei Eur J Mineral 16:126

Shannon RD (1976) Revised effective ionic radii and systematic studies of interatomic distances in halides and chalcogenides. Acta Crystallogr A32:751–767

Sheldrick G (1997) SHELX-97. A program for the refinement of crystal structures. Universität Göttingen, Germany

Song Y, Zavalij PY, Suzuki M, Whittingham MS (2002) New iron(III) phosphate phases: crystal structure, electrochemical and magnetic properties. Inorg Chem 41:5778–5786

Yonemura M, Yamada A, Takei Y, Sonoyama N, Kanno R (2004) Comparative kinetic study of olivine Li_xMPO_4 (M=Fe, Mn). J Electrochem Soc 151:A1352–A1356